Nuclear Instruments and Methods in Physics Research B 317 (2013) 77–82

Contents lists available at SciVerse ScienceDirect

Nuclear Instruments and Methods in Physics Research B

journal homepage: www.elsevier.com/locate/nimb

# Interaction potentials for multi-electron atoms in front of a LiF (001) surface from rainbow scattering

M.S. Gravielle [a], J.E. Miraglia [a,*], A. Schüller [b], H. Winter [b]

[a] Instituto de Astronomía y Física del Espacio (CONICET-UBA), Casilla de correo 67, sucursal 28, C1428EGA Buenos Aires, Argentina
[b] Institut für Physik, Humboldt Universität zu Berlin, Newtonstrasse 15, D-12489 Berlin-Adlershof, Germany

ARTICLE INFO

*Article history:*
Received 18 September 2012
Received in revised form 5 February 2013
Available online 19 February 2013

*Keywords:*
Rainbow scattering
Surface channeling
Surface eikonal approximation

ABSTRACT

Pairwise interaction potentials for multi-electron atoms moving in front of a LiF (001) surface are investigated theoretically and experimentally. From angular distributions of fast He, N, S, Cl and Kr atoms grazingly scattered under axial surface channeling conditions, rainbow angles are experimentally determined for a wide range of energies for the motion normal to the surface plane. These angles are used as a benchmark to probe the pairwise potential model. In the simulations the scattering process is described by means of the surface eikonal approximation, while the atom–surface interaction is derived by adding binary interatomic potentials that include the proper asymptotic limit.



## 1. Introduction

The atom–surface interaction potential plays a crucial role in the study of inelastic processes originated in grazing scattering of fast particles from solid surfaces. It determines the motion of the incident atoms above the surface, in the selvedge region where the electronic density displays a strong variation, affecting consequently electron emission yields, electronic excitation probabilities, projectile charge states, etc. In the case of ionic crystals, different models have been proposed to represent such an interaction [1–6]. Some of those fail to describe the angular distributions of swift atoms elastically scattered along low-indexed crystallographic directions (*axial surface channeling*) [7–9]. In particular, the angular positions of the outermost maxima of the projectile distribution, which result from rainbow scattering, were found to be sensitive to the corrugation of the surface potential across the incidence channel, becoming a useful tool to examine this interaction [10–12].

In this article we investigate the interaction potentials for multi-electron atoms – He, N, S, Cl and Kr – at a LiF (001) surface by using a pairwise additive model. The model is based on the sum of individual interatomic potentials, which take into account contributions from the different ionic centres of the insulator [13]. In this way, the binary potentials associated with the interaction between the atomic projectile and isolated $Li^+$ and $F^-$ ions become the elementary bricks used to build the atom–LiF surface potential. In previous works [14,15] we have derived He–$Li^+$and He–$F^-$ binary potentials by means of the Local Density Approximation (LDA), as given by the Abrahamson method [16]. For ionic materials, due to the high electron density localization around the atomic nuclei, this simple approach was found to be a good approximation for the description of grazing scattering processes [7,8,17], being a reliable alternative to self-consistent ab initio calculations. Here we explore a modification of the LDA to incorporate the Hartree–Fock (HF) limit values corresponding to the kinetic and exchange energies. In addition, the surface potential model includes also projectile polarization and surface rumpling, two effects that were found to be important for the description of fast atom diffraction patterns [14,18,15].

In order to test the potentials, we study experimentally and theoretically the angular positions of rainbow peaks for axial channeling. Results for two different directions of the LiF crystal – <110> and <100> – are analyzed in terms of the perpendicular incidence energy, considering values in the range 0.1–60 eV.

To describe the scattering process we employ a distorted-wave model – the surface eikonal approximation [14] – that makes use of the eikonal wave function to represent the elastic collision with the surface, while the motion of the fast projectile is classically described by considering axially channeled trajectories for different initial conditions. This method is a semi-classical approximation that includes a clear description of the main mechanisms of the process and has been successfully applied to investigate fast atom diffraction from insulator surfaces [15,17,19]. In comparison to other approaches [20,18,21], within the eikonal model the corrugation of the complete three dimensional surface potential is taken into account without averaging the projectile–surface interaction along the incidence direction. Inelastic processes, such as exciton

* Corresponding author.
*E-mail address:* miraglia@iafe.uba.ar (J.E. Miraglia).

0168-583X/$ - see front matter © 2013 Elsevier B.V. All rights reserved.
http://dx.doi.org/10.1016/j.nimb.2013.02.006

and electron production and electron transfer, are not considered in the present work. For helium projectiles (and for rare gases as well) these contributions are expected to be negligible [22], but for projectiles with open shells inelastic processes might play an important intermediate role not accounted in our scheme.

The experimental method and the theoretical formalism are summarized in Sections 2 and 3, respectively. Results are presented and discussed in Section 4, and in Section 5 we outline our conclusions. Atomic units ($e^2 = \hbar = m_e = 1$) are used unless otherwise stated.

## 2. Experiment

In our experiments we have scattered $^3$He, N, S, Cl, and Kr atoms with impact energies $E_i$ ranging from 3 keV to 70 keV from a LiF (001) surface under a grazing angle of incidence $\theta_i$. The angles of incidence were adjusted in such a manner that the energy for the motion of projectiles normal with respect to the surface plane $E_{i\perp} = E_i \sin^2\theta_i$ was between about 1 eV and 70 eV. The fast atoms were produced from ions generated in an ECR ion source via neutralization in a gas cell in the accelerator beam line. The neutralized beam was thereafter collimated by three sets of vertical and horizontal slits to a divergence of less than 0.03°. The adjustable slits are components of a two stage differential pumping system in order to maintain a base pressure in the $10-11$ mbar domain in our UHV scattering chamber. The target was prepared by cycles of grazing sputtering with 25 keV $Ar^+$ under $\theta_i \approx 2°$ at a target temperature of about 200 °C and subsequent annealing of the target at a temperature of 350 °C for about 15 min. After a major number of preparation cycles well defined angular distributions for scattered atoms were observed.

The azimuthal orientation of the LiF (001) surface was chosen such that the incident beam was directed along a <110> or <100> direction in the surface plane. The angular distributions were measured by means of a position sensitive micro-channel-plate detector which was mounted 0.66 m behind the target. With typical count rates of some 1000 counts per second, a complete angular pattern was recorded within a couple of minutes. As a representative example for our experimental data we show in Fig. 1 an angular distribution for the scattering of 70 keV Kr atoms from a LiF (001) surface along the <100> direction under a grazing angle of incidence $\theta_i = 1.4°$. The distribution is presented in a colour-coded 2D-plot (red = high intensity, blue = low intensity) and reveals three pronounced peaks which can be attributed to double scattering for the central peak and rainbow scattering for the two outer peaks. The rainbow angle $\Theta_{rb}$ is marked in the figure and will be used for comparison with the calculations presented here.

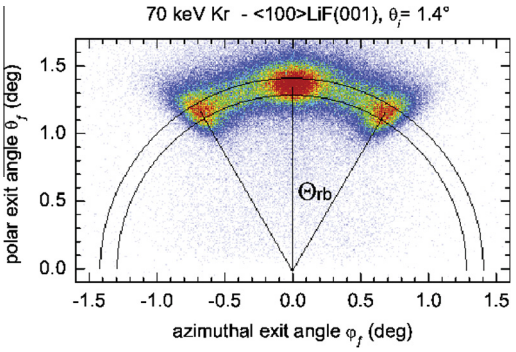


**Fig. 1.** Two dimensional intensity distribution, as recorded with a position sensitive detector, for Kr atoms scattered from LiF (001) along the ⟨100⟩channel. The incidence energy and angle are $E_i$= 70 keV and $\theta_i$=1.4°, respectively.

## 3. Theoretical model

When a swift atom impinges on a crystal surface under axial surface channeling conditions, the elastic scattering can be described by means of the surface-eikonal transition matrix [14], which reads:

$$T_{if}^{(eik)} = \frac{1}{\mathcal{A}} \int_{\mathcal{A}} d\vec{R}_{os}\; a_{if}(\vec{R}_{os}), \tag{1}$$

where $\vec{R}_{os}$ determines the initial position of the projectile on the surface plane, with $\mathcal{A}$ the integration area, and

$$a_{if}(\vec{R}_{os}) = \frac{1}{(2\pi)^3} \int_{-\infty}^{+\infty} dt \left| v_z(\vec{\mathcal{R}}_P) \right| \times \exp[-i\vec{Q}.\vec{\mathcal{R}}_P - i\eta(\vec{\mathcal{R}}_P)]\; V_{\rm surf}(\vec{\mathcal{R}}_P) \tag{2}$$

is the transition amplitude associated with the classical path $\vec{\mathcal{R}}_P = \vec{\mathcal{R}}_P(\vec{R}_{os}, t)$, with $v_z(\vec{\mathcal{R}}_P)$ being the component perpendicular to the surface plane of the projectile velocity at the time $t$. In Eq. (2), $\vec{Q} = \vec{K}_f - \vec{K}_i$ denotes the projectile momentum transfer, with $\vec{K}_{i(f)}$ the initial (final) projectile momentum satisfying the energy conservation, i.e. $K_f = K_i$. The phase $\eta$ is the eikonal-Maslov phase, which is defined along the projectile path as [19]

$$\eta(\vec{\mathcal{R}}_P) = \int_{-\infty}^{t} dt'\; V_{\rm surf}(\vec{\mathcal{R}}_P(t')) + \phi_M, \tag{3}$$

where $V_{\rm surf}$ is the projectile–surface interaction and $\phi_M = \nu\pi/2$ is the Maslov correction term, with $\nu$ the Maslov index as defined in Ref. [23].

Within the surface-eikonal model, the angular distribution of elastically scattered atoms can be derived from Eq. (1) as $dP/d\Omega_f = (2\pi)^4 m_P^2 \left| T_{if}^{(eik)} \right|^2$, where $m_P$ is the projectile mass and $\Omega_f$ is the solid angle corresponding to the exit direction of the projectile. This distribution depends strongly on $V_{\rm surf}$, which determines not only the eikonal phase but also the classical projectile trajectories.

### 3.1. The atom–surface interaction

In this work the projectile–surface potential is expressed by the sum of the static (short range) and polarization (long range) contributions, i.e.,

$$V_{\rm surf}(\vec{R}) = V_{\rm surf}^{(st)}(\vec{R}) + V_{\rm surf}^{(pol)}(\vec{R}), \tag{4}$$

where $\vec{R}$ is the projectile position vector. In Eq. (4), the static potential, $V_{\rm surf}^{(st)}$, represents the interaction between the atom and the crystal surface derived by assuming that their electronic densities remain frozen when the atom approaches the surface. The polarization term, $V_{\rm surf}^{(pol)}$, is due to the rearrangement of the projectile electron density induced by the presence of the ionic surface.

As we are dealing with an ionic insulator, where all electrons are strongly localized around the ionic nuclei, the static potential is evaluated by adding the individual interactions with solid ions, including the topmost and several atomic layers of the bulk (*pairwise additive* hypothesis). It reads

$$V_{\rm surf}^{(st)}(\vec{R}) = \sum_j V_{\rm bin}(\vec{R}_j), \tag{5}$$

where the sum formally includes all the ions of the target crystal, with $\vec{R}_j$ the position vector of the projectile with respect to the target ion labelled as $j$, and $V_{\rm bin}(\vec{R}_j)$ represents the binary interaction between the projectile and the target ion $j$.

In a similar way, the polarization potential is expressed as

$$V_{\rm surf}^{(pol)}(\vec{R}) = -\frac{C_4}{2}\left|\sum_j \frac{\widetilde{Z}(R_j)}{R_j^2}\widehat{R}_j\right|^2, \quad (6)$$

where $C_4$ is the atomic polarizability of the projectile [24], $\widehat{R}_j = \vec{R}_j/R_j$, and $\widetilde{Z}(R_j)$ is an effective charge which has been introduced to make each term of Eq. (6) finite at the origin. This effective charge is defined as [25]

$$\widetilde{Z}(R_j) = Z_{T_j}^{(\infty)}\left[1 - \left(1 + \frac{R_j}{R_0} + \frac{R_j^2}{2R_0^2}\right)\exp\left(-\frac{R_j}{R_0}\right)\right], \quad (7)$$

where $R_0$ is a screening parameter determined by the target and projectile mean radii, and $Z_{T_j}^{(\infty)}$ is the asymptotic ionic charge, with $Z_{T_j}^{(\infty)} = 1$ and $-1$ for $Li^+$ and $F^-$, respectively. In addition, in the evaluation of the static and polarization contributions we have considered a surface rumpling as reported in Ref. [19].

For the calculation of $V_{\rm bin}(\vec{R}_j)$, each binary projectile – solid ion potential was obtained from the Abrahamson model [16], which is equivalent to the Firsov method [26]. However, the original formalism has been modified in order to include the proper asymptotic limit of the kinetic and exchange contributions. Details on such calculations are explained in the following Subsection.

### 3.2. Binary static potentials

The short-range interaction between an atomic projectile $P$ and an ionic target $T_j$ can be approximated as a sum of three terms [16],

$$V_{\rm bin}(\vec{R}_j) = V_{\rm c}(\vec{R}_j) + V_{\rm k}(\vec{R}_j) + V_{\rm x}(\vec{R}_j), \quad (8)$$

corresponding to the Coulombic (c), kinetic (k) and exchange (x) potentials, respectively, where $\vec{R}_j$ is the relative position vector between the atomic nuclei. Note that in this expression we have omitted a fourth term, associated with the correlation potential, which is negligible in our case.

The first term of Eq. (8) represents the well known Coulomb interaction,

$$V_{\rm c}(\vec{R}_j) = \frac{Z_{T_j}Z_P}{R_j} - Z_{T_j}\int d\vec{r}\,'\,\frac{n_P(\vec{r}\,')}{|\vec{r}\,' + \vec{R}_j|} - Z_P\int d\vec{r}\,\frac{n_{T_j}(\vec{r})}{|\vec{r} - \vec{R}_j|} + \iint d\vec{r}\,d\vec{r}\,'\frac{n_P(\vec{r}\,')n_{T_j}(\vec{r})}{|\vec{R}_j - \vec{r} + \vec{r}\,'|}, \quad (9)$$

where $Z_P$ ($Z_{T_j}$) is the nuclear charge of $P$ ($T_j$), $n_P = n_P(\vec{r}\,')$ ($n_{T_j} = n_{T_j}(\vec{r})$) is the corresponding Clementi–Roetti electron density [27] as a function of the position vector $\vec{r}\,'$ ($\vec{r}$), which is measured with respect to its nucleus.

Within the Abrahamson method [16], the last two term of Eq. (8) can be evaluated under the assumption that the total density at any internuclear distance $R_j$ is given by its asymptotic form at large separations, that is,

$$n_{tot}(\vec{R}_j) = n_{T_j}(\vec{r}) + n_P(\vec{r} - \vec{R}_j). \quad (10)$$

Hence, the kinetic and exchange potentials read

$$V_{\rm k}(\vec{R}_j) = E_{\rm k}\left[n_{tot}(\vec{R}_j)\right] - E_{\rm k}\left[n_{T_j}\right] - E_{\rm k}[n_P],$$
$$V_{\rm x}(\vec{R}_j) = E_{\rm x}\left[n_{tot}(\vec{R}_j)\right] - E_{\rm x}\left[n_{T_j}\right] - E_{\rm x}[n_P], \quad (11)$$

where $E_{\rm k}[n]$ and $E_{\rm x}[n]$ are the kinetic and exchange energies, respectively, for a particle with a frozen electronic density $n$. By employing the Density Approximation [28], these energies can be expanded in terms of $n$ as

$$E_{\rm k}[n] = E_{\rm k}^{(1)}[n] + E_{\rm k}^{(2)}[n] + \ldots$$
$$E_{\rm x}[n] = E_{\rm x}^{(1)}[n] + E_{\rm x}^{(2)}[n] + \ldots \quad (12)$$

where the first orders, denoted by super-index (1), represent the local terms named LDA contributions, and the second orders, denoted by super-index (2), involve non local contributions depending on the gradient of the electronic density. The LDA kinetic and exchange energies read [16]

$$E_{\rm k}^{(1)}[n] = C_{\rm k}\int d\vec{r}\; n^{5/3}(\vec{r}),$$
$$E_{\rm x}^{(1)}[n] = C_{\rm x}\int d\vec{r}\; n^{4/3}(\vec{r}), \quad (13)$$

with $C_{\rm k} = 2.87123$ a.u. and $C_{\rm x} = -0.73856$ a.u. In Table 1 we present values of $E_{\rm k}^{(1)}$ and $E_{\rm x}^{(1)}$ for the ions and atoms of interest in the present article. They generally differ from the HF values $E_{\rm k}^{(\rm HF)}$ and $E_{\rm x}^{(\rm HF)}$ [28]; also shown in the Table. To a large extent the differences between the LDA and HF energy values are due to the contribution of the second and higher order terms in the expansion of Eq. (12) [28].

In this article we explore the possibility of improving $V_{\rm k}$ and $V_{\rm x}$ by including explicitly the intrinsic error involved in the LDA energies, as given by Eq. (13), contrasting them with the more accurate HF values. With this aim we quantize the error of the LDA energies by means of the ratios

$$\alpha[n] = \frac{E_{\rm k}^{(\rm HF)}[n]}{E_{\rm k}^{(1)}[n]}, \quad \beta[n] = \frac{E_{\rm x}^{(\rm HF)}[n]}{E_{\rm x}^{(1)}[n]}, \quad (14)$$

which are shown in Table 1. These parameters verify $\alpha[n] \cong \beta[n]$, in agreement with the recommendation by Lee et al. [29]. One simple way to account for these contributions is expressing the kinetic and exchange potentials in terms of *modified* total densities $n_{tot}^{(\rm k)}$ and $n_{tot}^{(\rm x)}$ as

$$V'_{\rm k}(\vec{R}_j) = E_{\rm k}\left[n_{tot}^{(\rm k)}(\vec{R}_j)\right] - E_{\rm k}^{(\rm HF)}\left[n_{T_j}\right] - E_{\rm k}^{(\rm HF)}[n_P],$$
$$V'_{\rm x}(\vec{R}_j) = E_{\rm x}\left[n_{tot}^{(\rm x)}(\vec{R}_j)\right] - E_{\rm x}^{(\rm HF)}\left[n_{T_j}\right] - E_{\rm x}^{(\rm HF)}[n_P], \quad (15)$$

where

$$n_{tot}^{(\rm k)}(\vec{R}_j) = \alpha_{T_j}^{3/5}\; n_{T_j}(\vec{r}) + \alpha_P^{3/5}\; n_P(\vec{r} - \vec{R}_j), \quad (16)$$

$$n_{tot}^{(\rm x)}(\vec{R}_j) = \beta_{T_j}^{3/4}\; n_{T_j}(\vec{r}) + \beta_P^{3/4}\; n_P(\vec{r} - \vec{R}_j), \quad (17)$$

to satisfy the proper asymptotic conditions, with $\alpha_\mu = \alpha[n_\mu]$ and $\beta_\mu = \beta[n_\mu]$ for $\mu = P, T_j$. At large $R_j$ distances, the potential $V'_{\rm k}$ ($V'_{\rm x}$) tends to one of Eq. (11) multiplied by a constant factor $\alpha_{T_j}(\beta_{T_j})$, which is equivalent to the $\alpha$X approximation introduced originally by Slater for exchange [30]. At this stage, it should be said that differences between the total density of Eq. (10) and the modified one given by Eq. (16) (Eq. (17)) are less than 2.5% (5%).

Finally, the *modified* binary potential introduced in this work extends Eq. (8) and reads

**Table 1**
Energies and parameters (in atomic units) of the binary interatomic potentials in the asymptotic limit, as explained in the text.

| Ion/Atom | $E_{\rm k}^{(1)}$ | $E_{\rm k}^{(\rm HF)}$ | $\alpha$ | $E_{\rm x}^{(1)}$ | $E_{\rm x}^{(\rm HF)}$ | $\beta$ |
|---|---|---|---|---|---|---|
| $Li^+$ | 6.544 | 7.236 | 1.106 | −1.420 | −1.651 | 1.162 |
| $F^-$ | 90.68 | 99.46 | 1.097 | −9.366 | −10.27 | 1.097 |
| He | 2.560 | 2.862 | 1.118 | −0.884 | −1.026 | 1.160 |
| N | 48.62 | 54.40 | 1.119 | −5.745 | −6.597 | 1.148 |
| S | 368.62 | 397.50 | 1.078 | −22.96 | −25.00 | 1.089 |
| Cl | 426.68 | 459.48 | 1.077 | −25.34 | −27.51 | 1.085 |
| Kr | 2590.9 | 2752.0 | 1.062 | −88.61 | −93.85 | 1.059 |

$$V'_{\rm bin}(\vec{R}_j) = V_{\rm c}(\vec{R}_j) + V'_{\rm k}(\vec{R}_j) + V'_{\rm x}(\vec{R}_j). \quad (18)$$

Note that this binary potential does not include any *ad hoc* parameter. Fig. 2(a) and (b) display $V'_{\rm bin}$, as defined in Eq. (18), for the interaction of all the projectiles considered in this article with $F^-$ and $Li^+$ ions, respectively. Results were plotted in terms of the absolute value of $V'_{\rm bin}(R_j) \times R_j(1+2R_j^3)$, in order to normalize the potential with the asymptotic limit, which is affected by the polarization. Inspecting the values of $\alpha$ and $\beta$ given in Table 1, we can estimate that the correction to $V_{\rm bin}(\vec{R}_j)$ introduced by the *modified* kinetic and exchange energies is of the order of very few percents, being 15% at most. However, as we are interested in collisions channeled along low-indexed crystallographic directions, rainbow angles are very sensitive to the corrugation of the potential at the turning point and this correction has to be investigated.

## 4. Results

We employ the angular distributions of fast atoms scattered from a LiF (001) surface along low-indexed crystallographic channels as a benchmark to probe the surface potential model. At the largest deflection angles, the angular projectile spectra present intense maxima, which are associated with rainbow scattering. We precisely focus on the rainbow angle $\Theta_{\rm rb}$, which is obtained from the final projectile distribution as the position of the outermost peaks expressed in terms of the deflection angle $\Theta$, defined as $\Theta = \arctan(\varphi_f/\theta_f)$, where $\theta_f$ and $\varphi_f$ are the polar and azimuthal exit angles, respectively (see Fig. 1).

In the geometry of axial channeling, the fast motion of the projectile parallel to the surface is weakly coupled to its much slower motion in the plane perpendicular to the surface. Consequently, rainbow angles depend only on the component of the impact energy associated with the motion perpendicular to the surface, $E_{i\perp}$. For He, N, S, Cl and Kr angular positions of rainbow peaks, as a function of $E_{i\perp}$, are displayed in Figs. 3–7, respectively, considering two incidence directions – <110> and <100>. In all the cases, the range of perpendicular energies extends up to 60 eV, except for He projectiles, for which the maximum is $E_{i\perp} = 10$ eV.

In Fig. 3, eikonal rainbow angles for He impact, derived by using the *modified* binary potentials of Eq. (18) to evaluate the pairwise surface interaction, are in very good accord with the experimental data in the considered range of perpendicular energies for the <110> channel and for $E_{i\perp} \gtrsim 0.2$ eV in the <100> direction. Similar level of agreement between theory and experiment is also

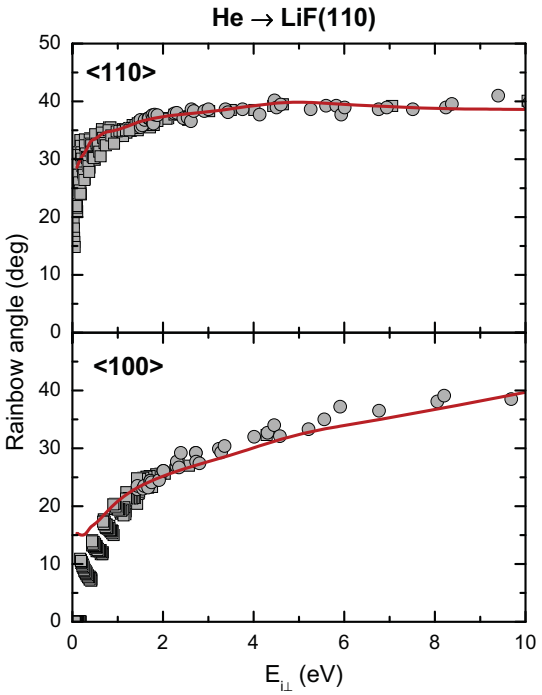


**Fig. 3.** (Color online) Rainbow angles $\Theta_{\rm rb}$, as a function of the perpendicular energy $E_{i\perp}$, for $^3$He atoms scattered from LiF (001) along the (a) ⟨110⟩and (b) ⟨100⟩directions, respectively. Solid symbols, experimental data for rainbow angles, different symbols corresponding to different total energies. Red solid line, eikonal results obtained by using a pairwise additive potential with *modified* binary interactions, as given by Eq. (18).

observed in Fig. 4 for scattering of N atoms along the <100> channel. However, for N projectiles impinging along the <110> direction eikonal results overestimate moderately the experimental rainbow angles for perpendicular energies lower than 25 eV, converging to the experiment as $E_{i\perp}$ increases.

Fairly good agreement between eikonal and experimental results is also found in Fig. 5 for S projectiles. For the <100> channel the eikonal curve runs below the experimental data as the energy increases, this deviation reaches about 11% at $E_{i\perp} = 60$ eV. In turn, for Cl projectiles (Fig. 6) the eikonal curves run near the experimental values for both crystallographic directions. In the <100> direction, differences between the theoretical and experimental

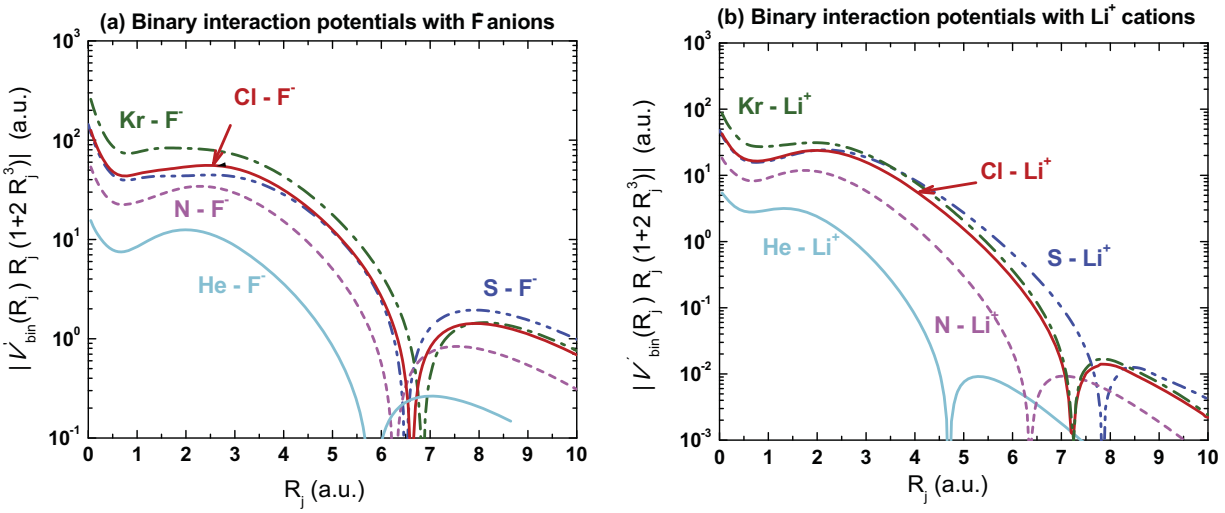


**Fig. 2.** (Color online) Binary interatomic potentials in atomic units, evaluated from Eq. (18), as a function of the internuclear distance $R_j$. (a) Absolute value of $V'_{bin}(R_j) \times R_j(1+2R_j^3)$ for binary interaction potentials with $F^-$ anions. (b) Similar to (a) for binary interaction potentials with $Li^+$ cations.

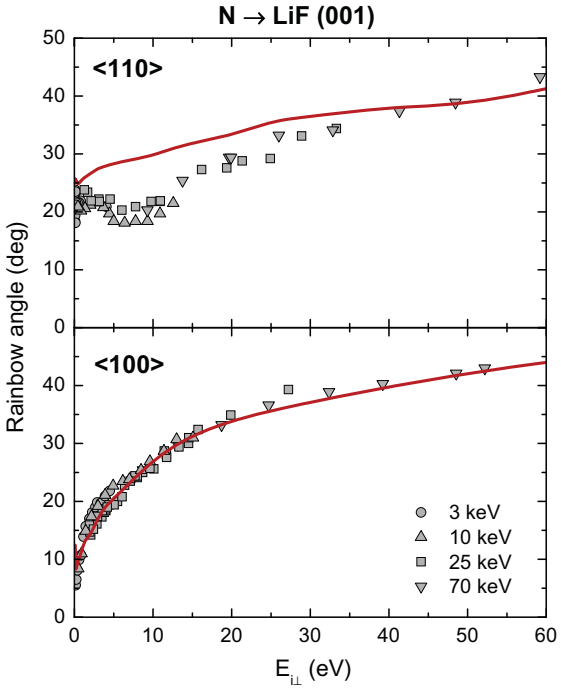


**Fig. 4.** Similar to Fig. 3 for N projectiles.

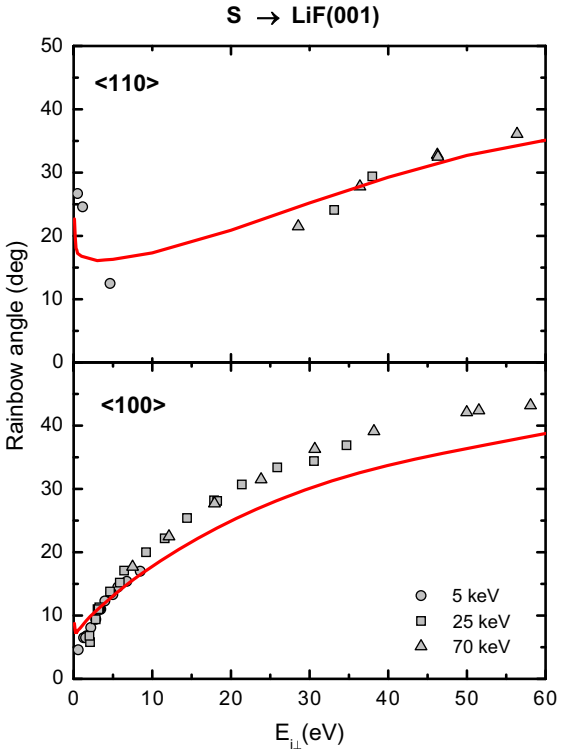


**Fig. 5.** Similar to Fig. 3 for S projectiles.

data at high perpendicular energies are lower than 10%. On the other hand, we should mention that the steep increase of eikonal rainbow angles at $E_{i\perp} \lesssim 0.8$ eV for the <1 1 0> channel, also observed for other projectiles, is affected by the screening of the polarization potential, as given by Eq. (7).

In Figs. 7 we display results for Kr. The agreement of the eikonal values with the experimental data is particularly remarkable for

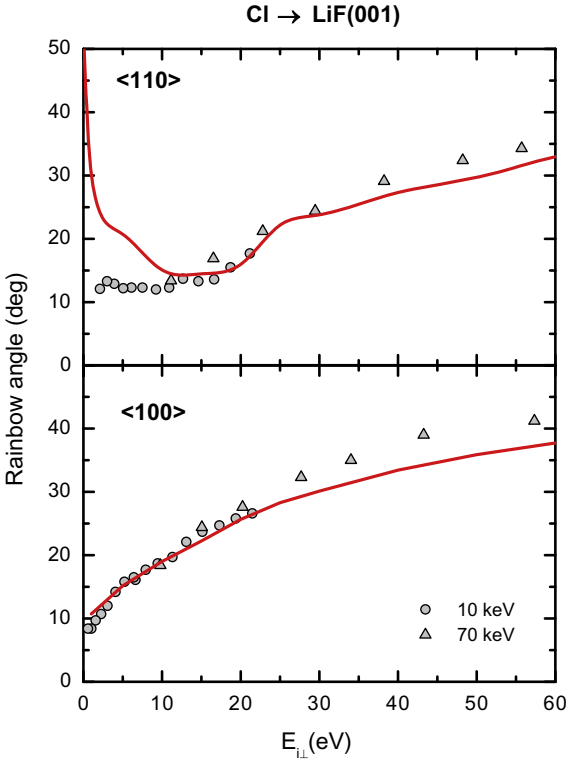


**Fig. 6.** Similar to Fig. 3 for Cl projectiles.

the <1 1 0> channel, for which experimental rainbow angles as a function of $E_{i\perp}$ show a slope change at intermediate perpendicular energies that is well reproduced by the theoretical model. Such a

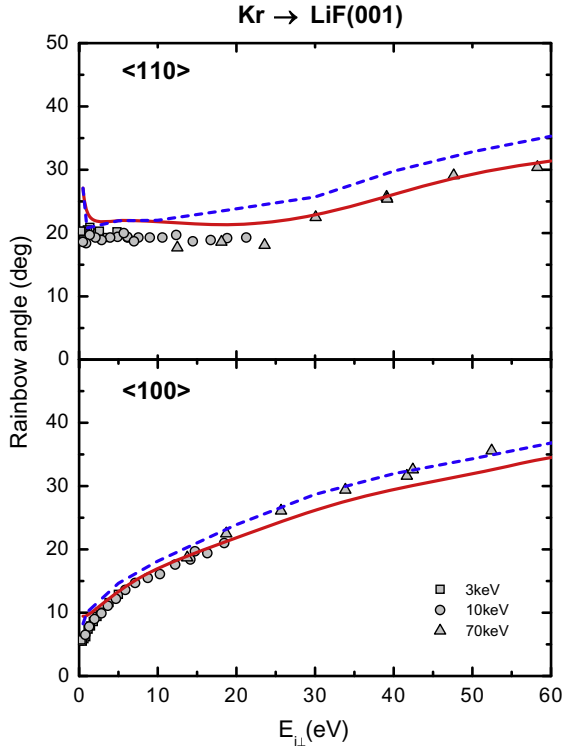


**Fig. 7.** Similar to Fig. 3 for Kr projectiles. Blue dashed line, eikonal results obtained by using a pairwise additive potential with LDA binary interactions, as given by Eq. (8)

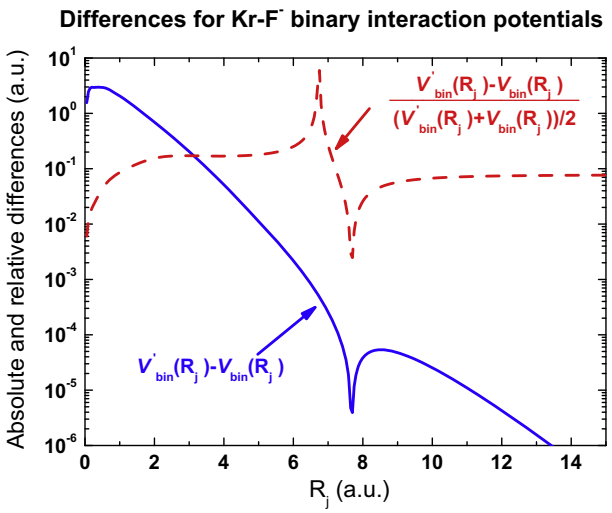


**Fig. 8.** (Color online) Differences between *modified* and original LDA binary potentials, as given by Eqs. (18) and (8), respectively, as a function of the internuclear distance $R_j$, for the Kr-$F^-$ interaction. Blue solid (red dashed) line, absolute (relative) difference between the binary potentials, as indicated by the label.

change of the slope, also observed for Cl, might be affected by the quantum–classical transition of the rainbow scattering process.

Taking into account that different perpendicular energies are probing the projectile–surface interaction for different distances to the surface, the overall good concordance of the theoretical results with the experimental positions of rainbow maxima is a clear indication of the quality of the proposed pairwise surface potential, which includes the proper asymptotic limit of the binary atom–ion interactions.

Finally, in order to investigate the differences introduced by the *modified* binary potential of Eq. (18), absolute and relative differences with the LDA binary potential, as given by Eq. (8), are shown in Fig. 8 for the case of the Kr–$F^-$ interaction. We focus the analysis on this projectile – Kr – because it is a multi-electron atom with a closed valence shell, which guarantees that additional open shell effects are not present. We found that the modification of the binary potential, as given by Eq. (18), introduces corrections between 8% and 20%, approximately (except, of course, around the zeros of the potential) in the LDA binary interaction. Similar differences are obtained for the other projectiles. But these differences produce only small corrections on the positions of rainbow angles (around 14%, at most), as illustrated in Fig. 7 where rainbow positions derived from the original LDA potential are plotted with a blue dashed line. Notice that in the case of the <100> direction, results obtained with the original LDA binary potential display a slightly better agreement with the experimental data at high normal energies than those derived with the *modified* form, while in the <110> direction the modified version is definitively more appropriate. However, the subject is open and we plan to study the contribution of terms of higher order in Eq. (12), as introduced by Becke [31] and Lee et al. [29].

## 5. Conclusions

From the agreement of eikonal results with experimentally observed rainbow angles we conclude that the pairwise additive potentials provide an appropriate description of the interaction of multi-electron atoms with a LiF (001) surface for perpendicular energies in the range from 1 to 60 eV. Here we have evaluated the binary interatomic potentials including information of the full HF values of the exchange and kinetics terms. Although these corrections were found to play a minor role in the rainbow scattering process, they might affect the positions of supernumerary rainbow maxima that arise as intermediate structures in the angular projectile distributions for low perpendicular energies [32].

We can summarize the following conclusions:

(i) No matter the considered projectile, at extremely low energies – lower than 0.2 – 0.8 eV – the pairwise additive model fails.
(ii) The potential model provides a very good description for impact of rare-gas atoms, including scattering of Ne projectiles investigated in a previous article [17].
(iii) We found a fairly good agreement for non-rare gas projectiles impinging along the <100> direction. The largest discrepancies are observed for S and Cl projectiles at high perpendicular energies, being the differences about 11% and 10%, respectively, at most. In this crystallographic direction the polarization is expected not to be relevant [14,17].
(iv) For scattering of Cl and N atoms along the <110> direction we found a large departure of the theory from the experimental data at low and intermediate normal energies. Notice that in contrast to rare gases, these projectiles have open shells, being an interesting point to focus our future research.

## Acknowledgment

M.S.G and J.E.M acknowledge financial support from CONICET, UBA, and ANPCyT of Argentina and H.W. from Deutsche Forschungsgemeinschaft (OFG).

## References

[1] J.F. Ziegler, J.P. Biersack, U. Littmark, The Stopping and Range of Ions in Solids, vol. 1, Pergamon Press, New York, 1985.
[2] D.J. O'Connor and J.P. Biersack, Nucl. Instrum. Methods Phys. Res. B, 15 (1986) 14.
[3] V. Celli, D. Eichenauer, A. Kaufhold, J.P. Toennies, J. Chem. Phys. 83 (1985) 2504.
[4] P.W. Fowler, J.M. Hutson, Phys. Res. B 33 (1986) 3724.
[5] D. Eichenauer, J.P. Toennies, Surf. Sci. 197 (1988) 267.
[6] D.J. Riley, A.P. Jardine, S. Dworski, G. Alexandrowicz, P. Fouquet, J. Ellis, W. Allison, J. Chem. Phys. 126 (2007) 104702.
[7] A. Schüller, K. Gärtner, H. Winter, Eur. Phys. Lett. 81 (2008) 37007.
[8] U. Specht, M. Busch, J. Seifert, A. Schüller, H. Winter, K. Gärtner, R. Wlodarczyk, M. Sierka, J. Sauer, Phys. Rev. B 84 (2011) 125440.
[9] U. Specht, M. Busch, J. Seifert, H. Winter, K. Gä rtner, R. Wlodarczyk, M. Sierka, J. Sauer, Nucl. Instrum. Methods Phys. Res. B, 269 (2011) 799.
[10] A. Schüller, H. Winter, Nucl. Instrum. Methods Phys. Res. B 267 (2009) 2621.
[11] J. Seifert, H. Winter, Surf. Sci. 603 (2009) L109.
[12] P. Tiwald, A. Schüller, H. Winter, K. Tökesi, F. Aigner, S. Gräfe, C. Lemell, J. Burgdörfer, Phys. Rev. B 82 (2010) 125453.
[13] A.J. García, J.E. Miraglia, Phys. Rev. A 74 (2006) 012902.
[14] M.S. Gravielle, J.E. Miraglia, Phys. Rev. A 78 (2008) 022901.
[15] M.S. Gravielle, J.E. Miraglia, Nucl. Instrum. Methods Phys. Res. B 267 (2009) 610.
[16] A.A. Abrahamson, Phys. Rev. 133 (1964) A990.
[17] M.S. Gravielle, A. Schüller, H. Winter, J.E. Miraglia, Nucl. Instrum. Methods Phys. Res. B 269 (2011) 1208.
[18] F. Aigner, N. Simonović, B. Solleder, L. Wirtz, J. Burgdörfer, Phys. Rev. Lett. 101 (2008) 253201.
[19] A. Schüller, H. Winter, M.S. Gravielle, J.M. Pruneda, J.E. Miraglia, Phys. Rev. A 80 (2009) 062903.
[20] A. Schüller, H. Winter, Phys. Rev. Lett. 100 (2008) 097602.
[21] A. Schüller, S. Wethekam, D. Blauth, H. Winter, F. Aigner, N. Simonović, B. Solleder, J. Burgdörfer, L. Wirtz, Phys. Rev. A 82 (2010) 062902.
[22] M. Bush, J. Lienemann, J. Seifert, A. Schuller, H. Winter, Vacuum 86 (2012) 1618.
[23] W.F. Avrin, R.P. Merrill, Surf. Sci. 311 (1994) 269.
[24] T.M. Miller, B. Bederson, Advances in Atomic and Molecular Physics, vol. 13, Academic, New York, 1977. pp. 1–55.
[25] K.T. Tang, J.P. Toennies, J. Chem. Phys. 80 (1984) 3726.
[26] O.B. Firsov, Zh. Eksp, Teor. Fiz. 32 (1957) 1464.
[27] E. Clementi, C. Roetti, Atom. Data Nucl. Data Tables 14 (1974) 177.
[28] J. Kohanoff, Electronic Structure Calculations for Solids and Molecules, Cambridge University Press, 2006.
[29] H. Lee, Ch. Lee, R.G. Parr, Phys. Rev. A 44 (1991) 768.
[30] J.C. Slater, Phys. Rev. 81 (1951) 385.
[31] A. Becke, Phys. Rev. A 38 (1988) 3098.
[32] H. Winter, A. Schüller, Prog. Surf. Sci. 86 (2011) 169.